Spin-orbit-induced magnetic anisotropy for impurities in metallic samples. II. Finite-size dependence in the Kondo resistivity

O. Újsághy
Institute of Physics and Research Group of Hungarian Academy of Sciences, Technical University of Budapest, H-1521 Budapest, Hungary

A. Zawadowski
Institute of Physics and Research Group of Hungarian Academy of Sciences, Technical University of Budapest, H-1521 Budapest, Hungary
and Research Institute for Solid State Physics, POB 49, H-1525 Budapest, Hungary

(Received 29 July 1997)

The electrical resistivity, including the Kondo resistivity increase at low temperature, is calculated for thin films of dilute magnetic alloys. Assuming that in the nonmagnetic host the spin-orbit interaction is strong like in Au and Cu, the magnetic impurities have a surface anisotropy calculated in paper I. That anisotropy hinders the motion of the spin. Including that anisotropy, the effective electron-impurity coupling is calculated by using the second-order renormalization-group equations. The amplitude of the Kondo resistivity contribution is reduced as the position of the impurity approaches the surface, but the increase occurs approximately at the bulk Kondo temperature. Different proximity effects are also explained qualitatively, where the films of magnetic alloys are covered by pure second films with different mean free path. The theory explains the experimental results in those cases, where a considerable amount of impurities is at the surface inside the ballistic region. [S0163-1829(98)05918-9]

I. INTRODUCTION

In the preceding paper,[1] (hereafter referred to as I) following Refs. 2 and 3, we have calculated the magnetic anisotropy for a magnetic impurity embodied into a nonmagnetic host (e.g., Au, Cu) with large spin-orbit interaction for the conduction electrons on the sites of the host atoms. The magnetic anisotropy is developed due to the exchange interaction between the magnetic impurities and the conduction electrons. As the scattering due to impurities involves different angular momentum channels ($-l<m<l$), the scattering therefore depends on the directions of the conduction electrons before and after the scattering. In this way, the scattering on the impurity itself depends on which host atoms the electrons are scattered by the spin-orbit interaction. Due to that dependence, the anisotropy is determined by the positions of host atoms around the impurity and it is larger the stronger the asymmetry around the impurity. As that information is carried by the momenta, therefore it is restricted to the atoms in the range of the elastic mean free path l_{el}. Thus the anisotropy can be developed only if the impurity is inside surface area of the thickness of the elastic mean free path (ballistic region of the surface). If the surface in that region is planelike, then the anisotropy energy is [see Eq. (1) of I (Ref. 1)]

$$H_a = K_d(\mathbf{nS})^2, \tag{1}$$

where **S** is the spin operator of the impurity, **n** is the normal direction of the experienced surface element, and K_d is the anisotropy constant depending apart from the oscillatory part like $1/d$ on the distance d, measured from the surface. Of course, if the ballistic region contains the more sophisticated part of the surface, then the determination of the direction and amplitude of the anisotropy is a more complex task. The oscillatory part decays faster than $1/d$, approaching the bulk part of the sample [see Eq. (B20b) in I].

In the surface area, the anisotropy energy leads to different splitting schema shown in Fig. 1, depending whether the spin S is an integer or half-integer. In this way the spin very nearby the surface freezes into a singlet or doublet considering the integer and half-integer cases, respectively. Thus at low enough temperature the spin shows no, or a restricted, dynamics. It is important to point out that the states $m=\pm\frac{1}{2}$ for $S=\frac{5}{2}$ cannot be replaced by a doublet of $S=\frac{1}{2}$. The spins are rather squeezed into planar states, as shown in Fig. 2.

Assuming that $K_d \gg T$, the integer spin does not contribute to the resistivity, contrary to the case of the half-integer spin, where the two lowest states contribute to the resistivity. The spin $S=\frac{1}{2}$ is, however, not affected by anisotropy. Thus different behaviors of the electrical resistivity can be expected, depending on the value of the spin. Considering impurities nearby the surface inside the ballistic region, more and more orbitals become active as the impurity positions approaching the bulk (see Fig. 3).

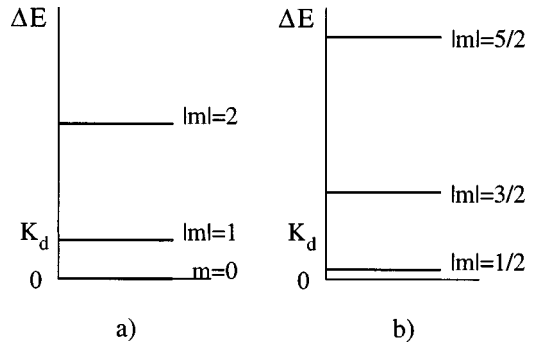

FIG. 1. The splitting schema due to the anisotropy for (a) $S=2$ and (b) $S=\frac{5}{2}$.

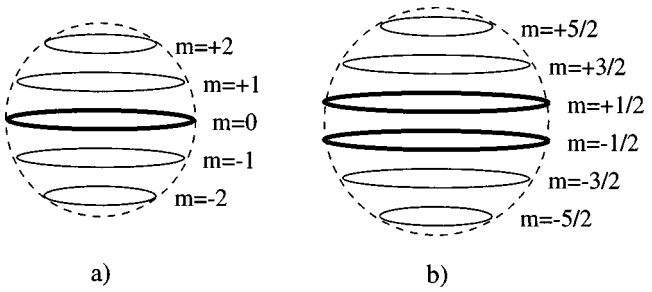

FIG. 2. The squeezing of the spin into planar states due to the anisotropy is illustrated for (a) $S=2$ and (b) $S=\frac{5}{2}$. The lowest-energy states are shown by heavy lines.

A similar structure appears in the temperature dependence of the resistivity. Cooling down the sample, at the beginning, almost all the spins are free. At further cooling, more and more spin states are frozen; thus when $S=2$ at $T<T_1$ three orbitals are populated, and when $T<T_2$, a single orbital is populated ($T_1:T_2=4:1$), while in case of $S=\frac{5}{2}$ each state is double degenerate ($T_1:T_2=25:9$).

Assuming that in the region of the Kondo temperature T_K the occupations of the different states are varying by a considerable amount depending on the positions of the impurities in the surface region, then, lowering the temperature, fewer and fewer impurities can further develop the Kondo state, and thus fewer and fewer impurities can contribute to a further increase of the Kondo resistivity. As has already been pointed out, the reduction in the contribution to the resistivity is somewhat less pronounced for a half-integer spin than for an integer spin (see the discussion of Fig. 2). The contribution to the Kondo resistivity can be schematically plotted for impurities with different distances measured from the surface $d_3<d_2<d_1$ (see Fig. 4).

The phenomena described above are very similar to the Kondo effect in the presence of a crystalline field at the impurity site. When lowering the temperature different crystal field states are frozen out, but those fields are identical for all impurities of the same kind. Such calculations have been performed, e.g., by Kashiba *et al.*[4]

The reduction in the averaged Kondo resistivity is sensitive to the size of the sample, e.g., the film thickness or diameter of the wire, etc., as the ratio of the surface-influenced impurities to the total number of impurities goes to zero as the size is further increased. The role of the surface on the impurities can be reduced by depositing another pure film on the surface of the sample. The effect can be also influenced by changing the elastic mean free path in the samples or in the deposited films. Effects of those kinds will be summarized and discussed at the end of the paper (see Sec. VII), making use the qualitative results obtained for the resistivity in Secs. V and VI, all of the references can be found there.

For the actual calculation of the resistivity, the temperature dependence of the effective exchange coupling must first be calculated. For that, except in the very low-temperature region, second-order multiplicative renormalization-group transformations (the two-loop approximation) can be used, which gives a smooth behavior at the Kondo temperature, in contrast to the first-order scaling

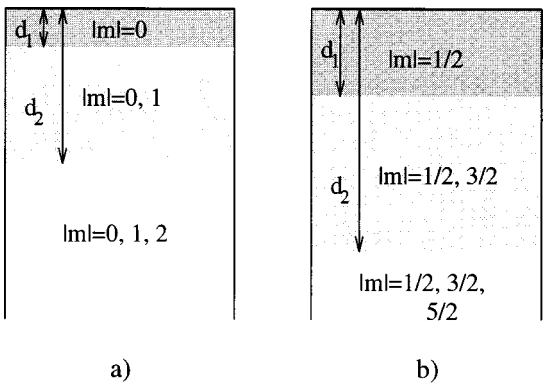

FIG. 3. The different layers of the impurity positions where more orbitals become active as the impurity positions approach the bulk assuming that $d_1, d_2 < l_{\mathrm{el}}$. (a) $S=2$, (b) $S=\frac{5}{2}$.

(one-loop approximation), which results in an artificial divergence at the Kondo temperature. Those methods are generalized by taking into account the surface anisotropy terms which occur as a low-energy cutoff of the logarithmic integrals in the calculation of certain diagrams. The different diagrams depending on their spin labels have a different infrared, low-energy cutoff due to the anisotropy. These calculations are in close analogy to those with crystalline splitting. The next step is using these effective couplings to calculate the electrical resistivity by solving the Boltzmann equation, and an average over the impurity positions is also taken.

Finally, to fit the calculated resistivity at low temperature, an effective surface layer thickness λ can be introduced, by assuming that inside of that surface region there is no Kondo effect, and outside the Kondo anomaly is fully developed. The experimental data are compared both with that phenomenological description and the original calculations, and they give equally excellent fits.

The paper is organized as follows. In Sec. II the general scheme of the multiplicative renormalization group (MRG) is presented for the Hamiltonian with the anisotropy term. The scaling equations are presented in Sec. III, and are solved in Sec. IV. The electrical resistivity contribution is calculated in Sec. V, and the dilute limit and Kondo resistivity in thin films are given in Sec. VI. Section VII is devoted to the experimental results, a theoretical interpretation of the results, and predictions. A general discussion is contained in Sec. VIII. The Appendix contains the actual calculation of the diagrams which are used in Sec. III. Throughout the paper, $\hbar=k_B=1$ units were used.

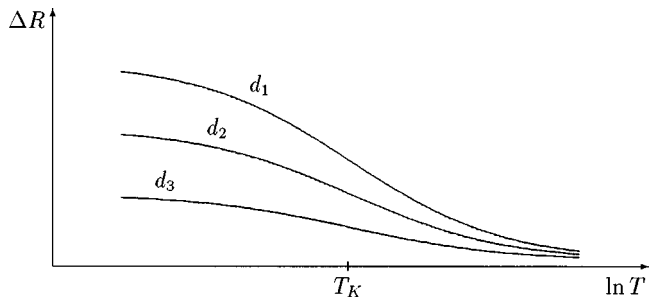

FIG. 4. The schematic plots of the contribution to the Kondo resistivity for impurities with different distances $d_3<d_2<d_1$ measured from the surface.

II. HAMILTONIAN AND THE GENERAL FORM OF THE MRG TRANSFORMATION

The Kondo Hamiltonian in the presence of the anisotropy is

$$H=\sum_{k,\sigma}\varepsilon_k a^\dagger_{k\sigma}a_{k\sigma}+H_a + \sum_{\substack{k,k',\sigma,\sigma'\\ M,M'}} J_{MM'}\boldsymbol{S}_{MM'}(a^\dagger_{k\sigma}\boldsymbol{\sigma}_{\sigma\sigma'}a_{k'\sigma'}), \tag{2}$$

where $a^\dagger_{k\sigma}$ ($a_{k\sigma}$) creates (annihilates) a conduction electron with momentum k, spin σ, and energy ε_k measured from the Fermi level. The conduction-electron band is taken with constant energy density ρ_0 for one spin direction, with a sharp and symmetric bandwidth cutoff D. $\boldsymbol{\sigma}$ stands for the Pauli matrices, $J_{MM'}$'s are the effective Kondo couplings, and H_a is given by Eq. (1). For the impurity spin, the Abrikosov' pseudofermion representation[5] was used,

$$\boldsymbol{S}=b^\dagger_M\boldsymbol{S}_{MM'}b_{M'}, \tag{3}$$

where the projections of the z component of the impurity spin are described by an auxiliary fermionic field b_M ($M=-S,\ldots,S$). Choosing the quantization axis parallel to **n**, with this substitution, the Hamiltonian Eq. (2) becomes

$$H=\sum_{k,\sigma}\varepsilon_k a^\dagger_{k\sigma}a_{k\sigma}+\sum_M(\lambda+K_M)b^\dagger_M b_M + \sum_{\substack{k,k',\sigma,\sigma'\\ M,M'}} J_{MM'}(b^\dagger_M\boldsymbol{S}_{MM'}b_{M'})(a^\dagger_{k\sigma}\boldsymbol{\sigma}_{\sigma\sigma'}a_{k'\sigma'}), \tag{4}$$

where the chemical potential $\lambda\to\infty$ was introduced to project out the physical pseudofermion subspace $\Sigma_M b^\dagger_M b_M=1$, and the notation $K_M=KM^2$ was introduced for the MRG calculation.

The conduction electron and pseudofermion Green's functions are

$$G_{k\sigma,k'\sigma'}(\omega)=\frac{\delta_{kk'}\delta_{\sigma\sigma'}}{\omega-\varepsilon_k-\Sigma_e} \tag{5}$$

and

$$\mathcal{G}_{MM'}(\tilde{\omega})=\frac{\delta_{MM'}}{\tilde{\omega}-\lambda-\Sigma_M(\tilde{\omega})}, \tag{6}$$

where $\tilde{\omega}=\omega-K_M$. Σ_e and $\Sigma_M(\tilde{\omega})$ are the self-energies for the conduction electrons and the pseudofermions, respectively. They are diagonal in adequate spin quantum numbers, and because of that the whole Hamiltonian is symmetric under rotation around the z axis. The vertex function is denoted by $\Gamma_{k\sigma M,k'\sigma'M'}(\omega_1,\omega_2,\omega_3,\omega_4)$.

The multiplicative renormalization group transformation can be written as[6]

$$G_{k\sigma,k'\sigma'}[\omega,J_{MM'}(D),K_M(D),D]=Z\left(\frac{D_0}{D}\right)G_{k\sigma,k'\sigma'}(\omega,J^0_{MM'},K^0_M,D_0), \tag{7a}$$

$$\mathcal{G}_{MM'}[\tilde{\omega},J_{\tilde{M}\tilde{M}'}(D),K_{\tilde{M}}(D),D]=Z_M\left(\frac{D_0}{D}\right)\mathcal{G}_{MM'}(\tilde{\omega},J^0_{\tilde{M}\tilde{M}'},K^0_{\tilde{M}},D_0), \tag{7b}$$

$$\Gamma_{k\sigma M,k'\sigma'M'}[\omega_i,J_{\tilde{M}\tilde{M}'}(D),K_{\tilde{M}}(D),D]=\frac{\Gamma_{k\sigma M,k'\sigma'M'}(\omega_i,J^0_{\tilde{M}\tilde{M}'},K^0_{\tilde{M}},D_0)}{Z\left(\frac{D_0}{D}\right)\sqrt{Z_M\left(\frac{D_0}{D}\right)}\sqrt{Z_{M'}\left(\frac{D_0}{D}\right)}}, \tag{7c}$$

where $Z(D_0/D)$ and $Z_M(D_0/D)$ are the renormalization factors for the electrons and pseudofermions, respectively. Introducing $x=\ln(D_0/D)$ as a scaling parameter, the Callan-Symantzik MRG equations are

$$-\eta G+\frac{\partial G}{\partial x}+\sum_{MM'}\beta_{MM'}\frac{\partial G}{\partial J_{MM'}}+\sum_M\gamma_M\frac{\partial G}{\partial K_M}=0, \tag{8a}$$

$$-\eta_M\mathcal{G}_M+\frac{\partial\mathcal{G}_M}{\partial x}+\sum_{\tilde{M}\tilde{M}'}\beta_{\tilde{M}\tilde{M}'}\frac{\partial\mathcal{G}_M}{\partial J_{\tilde{M}\tilde{M}'}}+\sum_{\tilde{M}}\gamma_{\tilde{M}}\frac{\partial\mathcal{G}_M}{\partial K_{\tilde{M}}}=0, \tag{8b}$$

$$\left(\eta+\frac{1}{2}\eta_M+\frac{1}{2}\eta_{M'}\right)\Gamma_{MM'}+\frac{\partial\Gamma_{MM'}}{\partial x}+\sum_{\tilde{M}\tilde{M}'}\beta_{\tilde{M}\tilde{M}'}\frac{\partial\Gamma_{MM'}}{\partial J_{\tilde{M}\tilde{M}'}}+\sum_{\tilde{M}}\gamma_{\tilde{M}}\frac{\partial\Gamma_{MM'}}{\partial K_{\tilde{M}}}=0, \tag{8c}$$

where

$$\eta=\frac{d\ln Z}{dx}, \tag{9a}$$

$$\eta_M=\frac{d\ln Z_M}{dx}, \tag{9b}$$

$$\beta_{MM'}=\frac{dJ_{MM'}}{dx}, \tag{9c}$$

$$\gamma_M=\frac{dK_M}{dx}, \tag{9d}$$

and for the sake of simplicity the electron and pseudofermion Green's function and the vertex function were denoted by G, $\mathcal{G}_M$, and $\Gamma_{MM'}$, respectively. The initial values for the renormalization factors and couplings are $Z=Z_M=1$, $K_M=K^{(0)}_M=KM^2$, and $J_{MM'}=J_0$ for each M, M' at $D=D_0$.

Using the definition of self-energies in Eqs. (5) and (6), the first two equations can be rewritten as

$$-(\omega-\varepsilon_k-\Sigma_e)\eta+\frac{\partial\Sigma_e}{\partial x}+\sum_{MM'}\beta_{MM'}\frac{\partial\Sigma_e}{\partial J_{MM'}}+\sum_M\gamma_M\frac{\partial\Sigma_e}{\partial K_M}=0, \tag{10a}$$

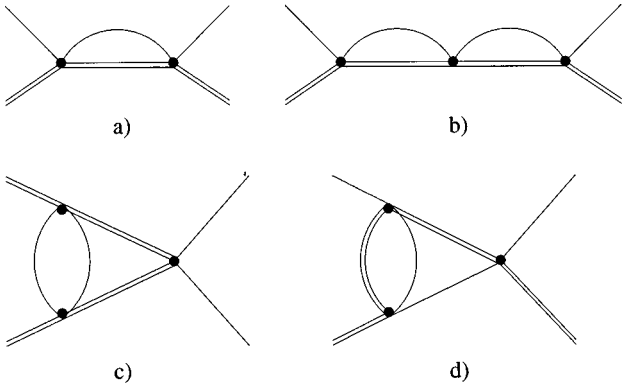

FIG. 5. The second- and third-order vertex corrections. The double line represents the impurity spin with the anisotropy energy, the single one represents the conduction electrons, and the solid circles stand for the exchange interaction.

$$-(\tilde{\omega}-\lambda-\Sigma_M)\eta_M+\frac{\partial\Sigma_M}{\partial x}+\sum_{\tilde{M}\tilde{M}'}\beta_{\tilde{M}\tilde{M}'}\frac{\partial\Sigma_M}{\partial J_{\tilde{M}\tilde{M}'}}+\sum_{\tilde{M}}\gamma_{\tilde{M}}\frac{\partial\Sigma_M}{\partial K_{\tilde{M}}}+\frac{dK_M}{dx}=0, \tag{10b}$$

the forms of which are more comfortable for calculating the MRG equations.

III. CONSTRUCTION OF THE MRG EQUATIONS

To construct the MRG equations the perturbation theory was applied; that is, the Hamiltonian was divided into noninteracting and interacting parts with small parameters $J_{MM'}$'s. When the electron self-energy contains a closed pseudofermion loop, Σ_e tends to zero as $\lambda\to\infty$. Thus in the thermodynamical limit, for a single impurity from Eq. (10a), $\eta=0$ and $Z=1$.

Turning to the other two equations (10b) and (8c), they were solved in a next-to-leading logarithmic approximation, where the MRG equations are

$$(\tilde{\omega}-\lambda)\eta_M^{(2)}=\frac{\partial\delta\Sigma_M^{(2)}}{\partial x}+\gamma_M^{(2)} \tag{11}$$

and

$$\frac{\partial\delta\Gamma^{(2)}_{\sigma M,\sigma' M'}}{\partial x}+\boldsymbol{\sigma}_{\sigma\sigma'}\boldsymbol{S}_{MM'}\beta^{(2)}_{MM'}=0, \tag{12a}$$

$$\left(\frac{1}{2}\eta_M^{(2)}+\frac{1}{2}\eta_{M'}^{(2)}\right)J_{MM'}\boldsymbol{\sigma}_{\sigma\sigma'}\boldsymbol{S}_{MM'}+\frac{\partial\delta\Gamma^{(3)}_{\sigma M,\sigma' M'}}{\partial x}$$

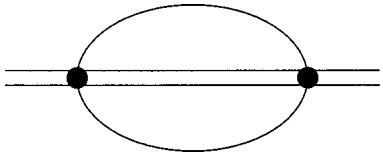

FIG. 6. The second-order self-energy correction for the impurity spin. The double line represents the impurity spin with the anisotropy energy, the single one represents the conduction electrons, and the solid circles stand for the exchange interaction.

$$+\sum_{\tilde{M}\tilde{M}'}\beta^{(2)}_{\tilde{M}\tilde{M}'}\frac{\partial\Gamma^{(2)}_{\sigma M,\sigma' M'}}{\partial J_{\tilde{M}\tilde{M}'}}+\boldsymbol{\sigma}_{\sigma\sigma'}\boldsymbol{S}_{MM'}\beta^{(3)}_{MM'}=0, \tag{12b}$$

where $\eta_M^{(2)}$, $\gamma_M^{(2)}$, and $\beta_{MM'}^{(2)}$ are proportional to the second power, and $\beta_{MM'}^{(3)}$ to the third power of the $J_{MM'}$'s, respectively. The whole next-to-leading logarithmic β function is $\beta_{MM'}=\beta_{MM'}^{(2)}+\beta_{MM'}^{(3)}$.

Thus, to construct the next-to-leading logarithmic scaling equations, we have to calculate the second- ($\delta\Gamma^{(2)}_{\sigma M,\sigma' M'}$) and third- ($\delta\Gamma^{(3)}_{\sigma M,\sigma' M'}$) order vertex corrections, and the second-order self-energy correction ($\delta\Sigma_M^{(2)}$) for the impurity spin.

These corrections were calculated by applying the thermodynamical Green's-function technique and an analytical continuation.[7] Assuming scaling for the vertex function $\Gamma_{MM'}$, only one energy variable was kept,[8] thus $\omega_1=\omega$, $\omega_2=K_M$, $\omega_3=\omega+K_M-K_{M'}$, and $\omega_4=K_{M'}$, where ω_1 and ω_2 are the incoming, and ω_3 and ω_4 the outgoing, electron and pseudofermion energies, respectively.

The second- and third-order vertex diagrams, and the second-order correction to the self-energy for the impurity spin, are shown in Figs. 5 and 6, respectively. A detailed calculation of these diagrams is carried out in the Appendix. Collecting all the second- and third-order vertex corrections together, they and the self-energy correction for the impurity spin were substituted into Eqs. (11) and (12). In Eq. (12b), the contributions of the third-order parquet-type diagrams depicted in Figs. 5(b) and 5(d) were canceled out with the terms $\Sigma_{\tilde{M}\tilde{M}'}\beta^{(2)}_{\tilde{M}\tilde{M}'}(\partial\Gamma^{(2)}_{\sigma M,\sigma' M'}/\partial J_{\tilde{M}\tilde{M}'})$, as the leading logarithmic scaling equations are equivalent to the summing up of the parquet diagrams. The divergences at finite T were also canceled out. Thus only Fig. 5(c) contributes to Eq. (12b).

Introducing the dimensionless couplings $j_{MM'}=\rho_0 J_{MM'}$, the next-to-leading logarithmic scaling equations are

$$\eta_M=\frac{d\ln Z_M}{dx}=q^2(S,M)j_{M,M-1}j_{M-1,M}\Theta_{M,M-1}(D)+p^2(S,M)j_{M,M+1}j_{M+1,M}\Theta_{M,M+1}(D)+2M^2j_{M,M}^2, \tag{13}$$

$$\gamma_M=\frac{dK_M}{dx}=(K_{M-1}-K_M)q^2(S,M)j_{M,M-1}j_{M-1,M}\Theta_{M,M-1}(D)+(K_{M+1}-K_M)p^2(S,M)j_{M,M+1}j_{M+1,M}\Theta_{M,M+1}(D), \tag{14}$$

$$\rho_0\beta_{M,M+1}=\frac{dj_{M,M+1}}{dx}=-[Mj_{M,M}-(M+1)j_{M+1,M+1}]j_{M,M+1}[1+\Theta_{M,M+1}(D)]$$
$$+q^2(S,M)j_{M,M-1}j_{M-1,M}j_{M,M+1}\Theta_{M,M-1}(D)[\Theta_{M,M+1}(D)-\tfrac{1}{2}]$$
$$+p^2(S,M+1)j_{M,M+1}j_{M+1,M+2}j_{M+2,M+1}\Theta_{M+1,M+2}(D)[\Theta_{M,M+1}(D)-\tfrac{1}{2}]$$
$$-p^2(S,M)j_{M,M+1}^2j_{M+1,M}\Theta_{M,M+1}(D)-M^2j_{M,M}^2j_{M,M+1}-(M+1)^2j_{M+1,M+1}^2j_{M,M+1}$$
$$+2M(M+1)j_{M,M}j_{M,M+1}j_{M+1,M+1}, \tag{15}$$

$$\rho_0\beta_{M,M-1}=\frac{dj_{M,M-1}}{dx}=-[(M-1)j_{M-1,M-1}-Mj_{M,M}]j_{M,M-1}[1+\Theta_{M,M-1}(D)]$$
$$+p^2(S,M)j_{M,M+1}j_{M+1,M}j_{M,M-1}\Theta_{M,M+1}(D)[\Theta_{M,M-1}(D)-\tfrac{1}{2}]$$
$$+q^2(S,M-1)j_{M,M-1}j_{M-1,M-2}j_{M-2,M-1}\Theta_{M-1,M-2}(D)[\Theta_{M,M-1}(D)-\tfrac{1}{2}]$$
$$-q^2(S,M)j_{M,M-1}^2j_{M-1,M}\Theta_{M,M-1}(D)-M^2j_{M,M}^2j_{M,M-1}-(M-1)^2j_{M-1,M-1}^2j_{M,M-1}$$
$$+2M(M-1)j_{M,M}j_{M,M-1}j_{M-1,M-1}, \tag{16}$$

and, for $M\neq 0$,

$$\rho_0\beta_{M,M}=\frac{dj_{M,M}}{dx}=\frac{1}{M}[q^2(S,M)\Theta_{M,M-1}(D)j_{M,M-1}j_{M-1,M}-p^2(S,M)\Theta_{M,M+1}(D)j_{M,M+1}j_{M+1,M}]$$
$$+q^2(S,M)\frac{M-1}{M}j_{M,M-1}j_{M-1,M-1}j_{M-1,M}\Theta_{M,M-1}(D)+p^2(S,M)\frac{M+1}{M}j_{M,M+1}j_{M+1,M+1}j_{M+1,M}\Theta_{M,M+1}(D)$$
$$-q^2(S,M)j_{M,M-1}j_{M-1,M}j_{M,M}\Theta_{M,M-1}(D)-p^2(S,M)j_{M,M+1}j_{M+1,M}j_{M,M}\Theta_{M,M+1}(D), \tag{17}$$

where $\Theta_{MM'}(D)$ ensures that $D>\sqrt{(K_M-K_{M'})^2+T^2}$, with the definition

$$\Theta_{MM'}(D)=\begin{cases}1 & \text{if } D>\sqrt{(K_M-K_{M'})^2+T^2}\\ 0 & \text{if } D<\sqrt{(K_M-K_{M'})^2+T^2}.\end{cases} \tag{18}$$

The definitions of $p(S,M)$ and $q(S,M)$ are given in Eq. (A7). It must be stressed that these scaling equations are valid for $T\leqslant D$.

IV. SOLUTION OF THE SCALING EQUATIONS

It can be seen from Eq. (14) that the corrections to the bare $K_M^{(0)}$ are proportional to the second power of $j_{MM'}$'s in the leading order. In the other equations, K_M appears only in the arguments of the Θ functions, which are multiplied by the second or third power of $J_{MM'}$'s. Thus to keep the approximation consistent, $K_M=K_M^{(0)}=KM^2$ can be taken in the arguments of the Θ functions. After this consideration, the solution of the equations becomes simpler, because the equations for $\beta_{MM'}$ are not coupled. Exploiting the symmetries of the scaling equations,

$$j_{M,M'}=j_{M',M}, \tag{19a}$$

$$j_{M,M'}=j_{-M,-M'} \tag{19b}$$

must hold.

Thus the equations which have to be solved are

$$\frac{dj_{M,M+1}}{dx}=-[Mj_{M,M}-(M+1)j_{M+1,M+1}]j_{M,M+1}[1+\Theta_{M,M+1}(D)]+q^2(S,M)j_{M,M-1}^2j_{M,M+1}\Theta_{M,M-1}(D)[\Theta_{M,M+1}(D)$$
$$-\tfrac{1}{2}]+p^2(S,M+1)j_{M,M+1}j_{M+1,M+2}^2\Theta_{M+1,M+2}(D)[\Theta_{M,M+1}(D)-\tfrac{1}{2}]-p^2(S,M)j_{M,M+1}^3\Theta_{M,M+1}(D)$$
$$-M^2j_{M,M}^2j_{M,M+1}-(M+1)^2j_{M+1,M+1}^2j_{M,M+1}+2M(M+1)j_{M,M}j_{M,M+1}j_{M+1,M+1}, \tag{20}$$

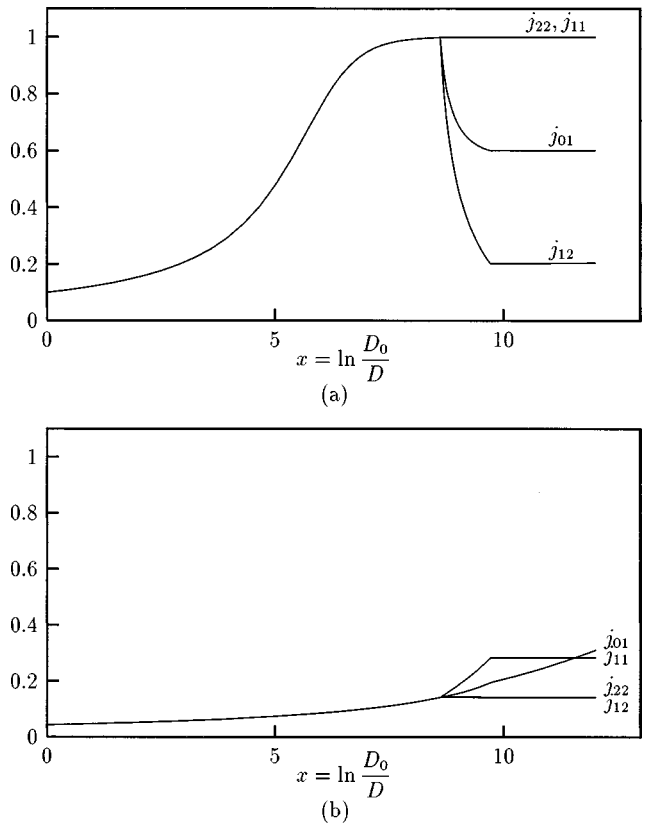

FIG. 7. The running couplings for $S=2$ as a function of $x=\ln(D_0/D)$ at $K=6$ K and $T=0.6$ K, with parameters $D_0=10^5$ K, (a) $j_0=0.1$, and (b) $j_0=0.0435$.

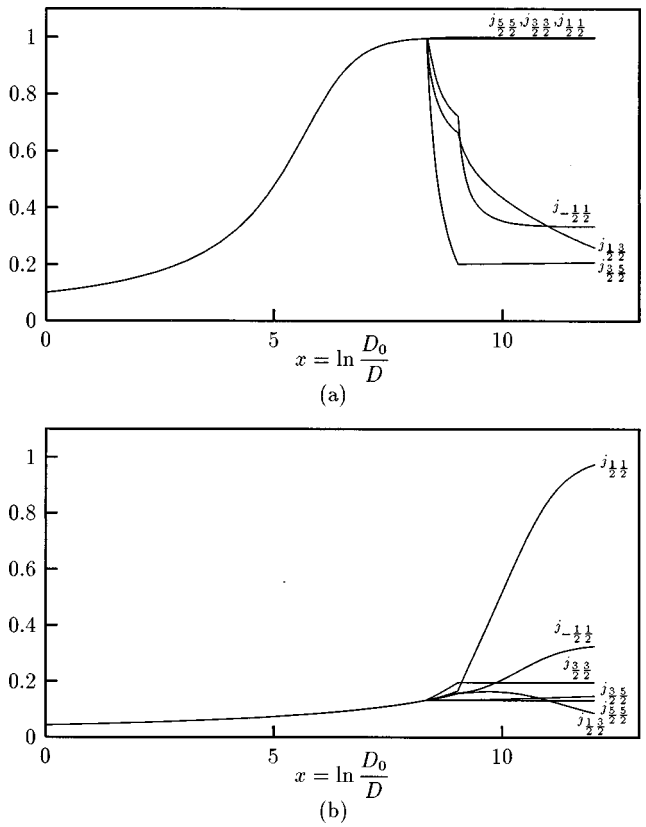

FIG. 8. The running couplings for $S=\frac{5}{2}$ as a function of $x=\ln(D_0/D)$ at $K=6$ K and $T=0.6$ K, with parameters $D_0=10^5$ K, (a) $j_0=0.1$, and (b) $j_0=0.0435$.

and, for $M\neq 0$,

$$\begin{aligned}\frac{dj_{M,M}}{dx}=&\frac{1}{M}[q^2(S,M)\Theta_{M,M-1}(D)j^2_{M,M-1}\\&-p^2(S,M)\Theta_{M,M+1}(D)j^2_{M,M+1}]\\&+q^2(S,M)\frac{M-1}{M}j^2_{M,M-1}j_{M-1,M-1}\Theta_{M,M-1}(D)\\&+p^2(S,M)\frac{M+1}{M}j^2_{M,M+1}j_{M+1,M+1}\Theta_{M,M+1}(D)\\&-q^2(S,M)j^2_{M,M-1}j_{M,M}\Theta_{M,M-1}(D)\\&-p^2(S,M)j^2_{M,M+1}j_{M,M}\Theta_{M,M+1}(D).\end{aligned}\tag{21}$$

These equations were solved numerically for different initial couplings $j_0=j_{MM'}(D=D_0)$. The results for $j_0=0.1$ and $j_0=0.0435$ at $K/T=10$ are shown in Figs. 7 and 8 for $S=2$ and $\frac{5}{2}$, respectively. The initial bandwidth cutoff was chosen as $D_0=10^5$ K.

V. RESISTIVITY

The Kondo resistivity was calculated by solving the Boltzmann equation in the presence of the spin-orbit-induced anisotropy, using the value of running couplings ($j_{MM'}$) calculated in Sec. IV, at $D=T$.

Taking the usual form[9] for the electron distribution function $f(\varepsilon_k)$ for both spin directions in the presence of the electric field **E** as

$$f(\varepsilon_k)=f_0(\varepsilon_k)-(\mathbf{kE})\Phi(\varepsilon_k)\frac{\partial f_0(\varepsilon_k)}{\partial\varepsilon_k},\tag{22}$$

the Kondo contribution to the resistivity is

$$\frac{1}{\rho_{\text{Kondo}}}=-\frac{e}{3\pi^2}(2m)^{3/2}\int d\varepsilon_k\varepsilon_k^{3/2}\Phi(\varepsilon_k)\left(-\frac{\partial f_0}{\partial\varepsilon_k}\right),\tag{23}$$

where the function Φ is determined by the Boltzmann equation

$$\frac{e}{m}\frac{\partial f_0(\varepsilon_k)}{\partial\varepsilon_k}(\mathbf{kE})+\left(\frac{\partial f}{\partial t}\right)_{\text{coll.}}=0.\tag{24}$$

The collision term $(\partial f/\partial t)_{\text{coll.}}$ can be expressed in terms of transition probabilities as

$$\begin{aligned}\left(\frac{\partial f}{\partial t}\right)_{\text{coll.}}=&\frac{c}{V}\sum_{\mathbf{k}'\sigma'}\{W(\mathbf{k}',\sigma'\rightarrow\mathbf{k},\sigma)f(\mathbf{k}')[1-f(\mathbf{k})]\\&-W(\mathbf{k},\sigma\rightarrow\mathbf{k}',\sigma')f(\mathbf{k})[1-f(\mathbf{k}')]\},\end{aligned}\tag{25}$$

where e.g., $W(\mathbf{k}',\sigma'\rightarrow\mathbf{k},\sigma)$ represents the transition probability from a $\mathbf{k}',\sigma'$ state to a $\mathbf{k}$, σ state, c is the impurity concentration, and V is the volume.

Turning to our case, these probabilities can be calculated as

$$W(\mathbf{k},\sigma\rightarrow\mathbf{k}',\sigma')=\sum_{MM'} p_M w(\mathbf{k},\sigma,M\rightarrow\mathbf{k}',\sigma',M'), \tag{26}$$

where

$$w(\mathbf{k},\sigma,M\rightarrow\mathbf{k}',\sigma',M') = 2\pi|T_{\mathbf{k},\sigma,M\rightarrow\mathbf{k}',\sigma',M'}|^2\delta(\varepsilon_k-\varepsilon_{k'}+KM^2-KM'^2), \tag{27}$$

and $p_M=e^{-\beta KM^2}/Z$, $\beta=1/T$, $Z=\Sigma_M e^{-\beta KM^2}$.

The scattering amplitude in Eq. (27) is expressed in terms of the renormalized couplings $J_{MM'}(x)$ as

$$T_{\mathbf{k},\sigma,M\rightarrow\mathbf{k}',\sigma',M'}\approx J_{MM'}\left(x=\ln\frac{D_0}{T}\right)\boldsymbol{\sigma}_{\sigma\sigma'}\boldsymbol{S}_{MM'}, \tag{28}$$

where the dependence on the direction of the momenta **k** and **k**′ is ignored, and that makes the Boltzmann equation solvable in a simple form. The k dependence may result as some numerical factors in the final expression, but in the main features of the temperature dependence those do not play an important role.

Substituting these assumptions into Eq. (25), changing the sum $(1/V)\Sigma_{k'}$ to $\int\rho(\varepsilon_{k'})d\varepsilon_{k'}\int(d\Omega_{k'}/4\pi)\approx\rho_0\int_{-D_0}^{D_0}d\varepsilon\int(d\Omega_{k'}/4\pi)$, using the properties of the spin algebra for $\boldsymbol{\sigma}$ and $\boldsymbol{S}$, and the ''detailed balance'' principle ($[\partial f_0(\varepsilon_k)/\partial t]_{\text{coll.}}=0$), we obtain, after linearization in **E**,

$$\left(\frac{\partial f}{\partial t}\right)_{\text{coll.}}=\frac{2\pi c}{\rho_0}(\mathbf{kE})\Phi(\varepsilon_k)\frac{\partial f_0}{\partial\varepsilon_k}F(\varepsilon_k), \tag{29}$$

where

$$F(\varepsilon_k)=\sum_M p_M\left\{M^2 j_{M,M}^2\left(x=\ln\frac{D_0}{T}\right)+[S(S+1)-M(M+1)]j_{M,M+1}^2\left(x=\ln\frac{D_0}{T}\right)\times\{1-(1-e^{-(2M+1)K/T})f_0[\varepsilon_k-(2M+1)K]\}\right\}, \tag{30}$$

where we introduced the dimensionless coupling constants $j_{MM'}=\rho_0 J_{MM'}$. Inserting Eq. (29) into the Boltzmann equation (24), we obtain, for Φ,

$$\Phi(\varepsilon_k)=-\frac{e}{m}\left[\frac{2\pi c}{\rho_0}F(\varepsilon_k)\right]^{-1}, \tag{31}$$

and, for the Kondo resistivity,

$$\frac{1}{\rho_{\text{Kondo}}}=\frac{1}{\rho^{(0)}}\int d\varepsilon\left(-\frac{\partial f_0}{\partial\varepsilon}\right)F^{-1}(\varepsilon), \tag{32}$$

where the usual assumption

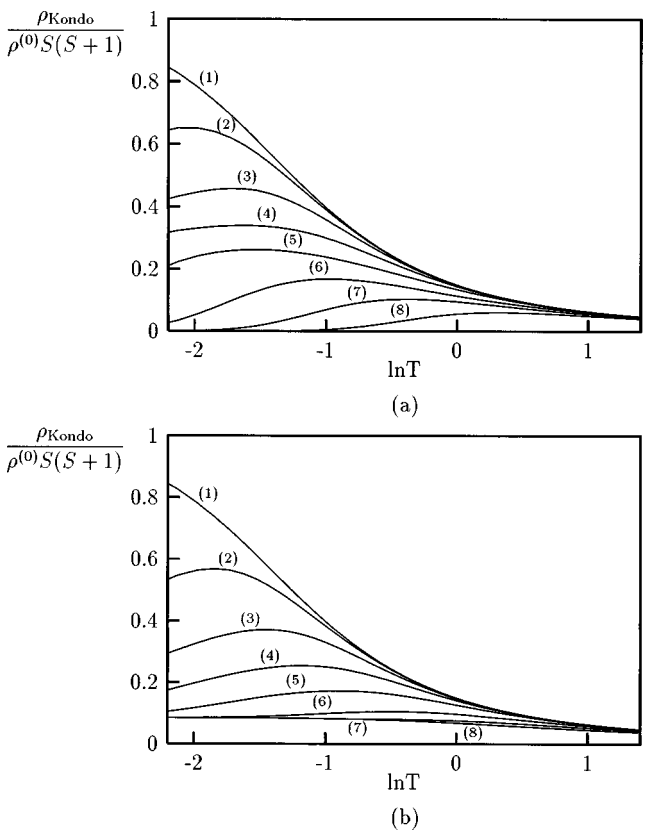

FIG. 9. The resistivity for (a) $S=2$ and (b) $S=\frac{5}{2}$ for different values of K. (1) $K=0$, (2) $K=0.02$ K, (3) $K=0.05$ K, (4) $K=0.1$ K, (5) $K=0.2$ K, (6) $K=0.5$ K, (7) $K=1$ K, and (8) $K=2$ K. The initial parameters were chosen as $j_0=0.0435$, $D_0=10^5$ K, and $T_K=0.3$ K.

$$\int d\varepsilon\,\varepsilon^{3/2}\left(-\frac{\partial f_0}{\partial\varepsilon}\right)F^{-1}(\varepsilon)\approx\varepsilon_F^{3/2}\int d\varepsilon\left(-\frac{\partial f_0}{\partial\varepsilon}\right)F^{-1}(\varepsilon) \tag{33}$$

was taken into account, and the constant $\rho^{(0)}=\frac{3}{4}(m/e^2)(2\pi c/\varepsilon_F\rho_0^2)$ was introduced. In the case of $K=0$, Eq. (32) reproduces the bulk Kondo resistivity.

The resistivity was calculated by evaluating the integral occurring in Eq. (32) numerically for different K values which are in the regime discussed in I.[1] The resistivity as the function of the temperature is shown in Figs. 9(a) and 9(b) for $S=2$ and $\frac{5}{2}$, respectively. The plots are similar to the experimental ones (see Sec. VII).

The effect of the anisotropy on the Kondo temperature defined by the largest slope in the resistivity can be examined by looking at the derivative of the calculated resistivity vs temperature. We can see from Figs. 9(a) and 9(b) that the Kondo temperature defined in that way is only slightly affected by the anisotropy in those cases where the Kondo effect is pronounced (e.g., $K<0.5$ K in Fig. 9). The effect of the anisotropy becomes dominant for larger strengths of K. The temperature dependence of the resistivity has a maximum depending on the strength of K, and the spin-flip contribution freezes out gradually. That behavior is very different for integer and half-integer spins for large anisotropy. For integer spins the impurity contribution tends to zero in a way which is very sensitive to the strength of the anisotropy. In the case of half-integer spins, however, the impurity resis-

tivity approaches a finite value at zero temperature which is independent of K. The resistivity there is determined by the dynamics of the two lowest-energy levels shown in Fig. 2. In those cases the Kondo effect is also essentially reduced due to the smallness of the spin-flip amplitudes, but still presents. (The Kondo contribution in the lowest order is proportional to $\boldsymbol{S\sigma}$ which gives a small amplitude for $M=\pm\frac{1}{2}$.) It is important to emphasize that, when $S=\frac{1}{2}$, the anisotropy loses its meaning.

In a real system the anisotropy strength K has a distribution; thus the formation of the resistivity maximum at a finite value of temperature cannot be expected at least above the Kondo temperature. The calculation is not reliable for $T<T_K$ in any case.

VI. KONDO RESISTIVITY IN THIN FILMS

To obtain some information about the case of thin films, a simple assumption is made that the two surfaces contribute to the anisotropy constant K in an additive way. The anisotropy factor for a sample with thickness t and in a distance d measured from one of the surfaces is

$$K(d,t)=K_d+K_{t-d}=\frac{\alpha}{d}+\frac{\alpha}{t-d}, \tag{34}$$

where the coefficient α is estimated in I (Ref. 1) [see Eq. (32)]. The appropriate calculation of the resistivity including the elastic impurity scattering with mean free path $l_{\rm el}$ is a very difficult task for a film for an arbitrary ratio of $l_{\rm el}/t$ and a value of K. In order to avoid those difficulties, we make use of the fact that the magnetic exchange (Kondo) contribution to the resistivity $\rho_{\rm Kondo}$ is smaller by a factor 10^{-3} than the residual normal impurity resistivity $\rho_{\rm nor}$ ($\rho=\rho_{\rm nor}+\rho_{\rm Kondo}$); thus an expansion in the Kondo contribution is appropriate. The calculation can be carried out in two limits (i) $t<l_{\rm el}$ and (ii) $t\gg l_{\rm el}$. It will be shown that the final expression does not depend on which limit is considered. In case (i), the electrical resistivity contains the average value of the inverse electron lifetime. Denoting the resistivity at temperature T for a given value of K by $\rho(K,T)$, the average over the value of $K(d,t)$ is

$$\overline{\rho}(t,T)=\frac{1}{t}\int_0^t \rho[K(x,t),T]dx. \tag{35}$$

On the other hand, in case (ii) the sample can be considered as a set of parallel resistors of equal size, where each resistor represents a stripe in the sample with a constant K. In that case the conductances are additive, thus

$$\overline{\rho}(t,T)=\frac{1}{\sigma_{\rm nor}+\frac{1}{N}\sum_i \sigma_i[K(x_i,t),T]}, \tag{36}$$

where N is the number of the resistors (stripes) labeled by i, and σ_i represents the Kondo conductivity of stripe i placed at a distance x_i. In the actual case only the first stripes depend on the surface anisotropy. The Kondo conductivity is defined by the Kondo resistivity given by Eq. (32) as

$$\sigma=\sigma_{\rm nor}+\sigma_{\rm Kondo}=(\rho_{\rm nor}+\rho_{\rm Kondo})^{-1}, \tag{37}$$

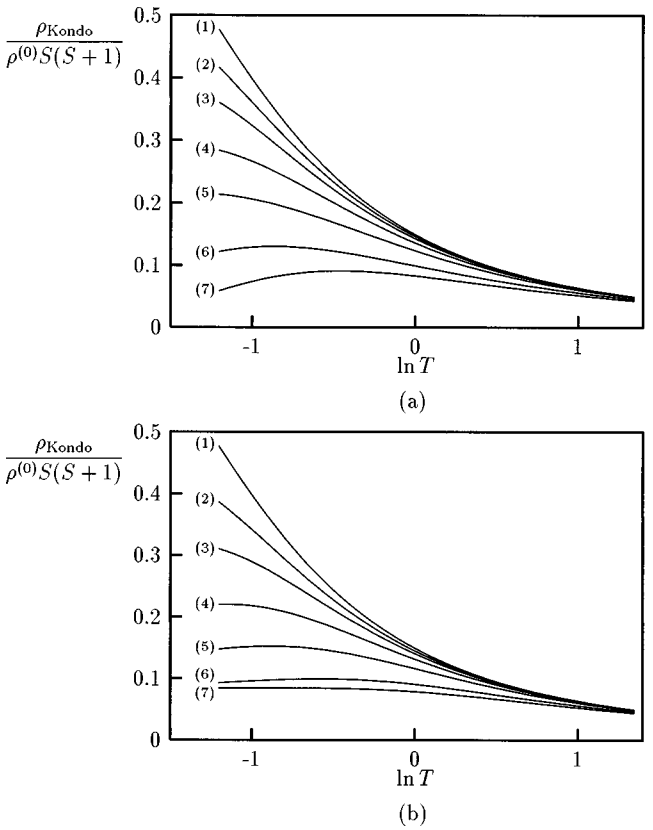

FIG. 10. The resistivity for (a) $S=2$ and (b) $S=\frac{5}{2}$ for different values of t/α. (1) $t/\alpha=\infty(K=0)$, (2) $t/\alpha=200(1/K)$, (3) $t/\alpha=100(1/K)$, (4) $t/\alpha=50(1/K)$, (5) $t/\alpha=25(1/K)$, (6) $t/\alpha=10(1/K)$, and (7) $t/\alpha=6(1/K)$. The initial parameters were chosen as $j_0=0.0435$, $D_0=10^5$ K, and $T_K=0.3$ K.

where $\sigma_{\rm Kondo}\approx-\rho_{\rm Kondo}/\rho_{\rm nor}^2<0$. The expansion gives the final expression

$$\overline{\rho}(t,T)=\rho_{\rm nor}+\frac{1}{t}\int_0^t \rho_{\rm Kondo}[K(x,t),T]dx. \tag{38}$$

That expression valid in the limit where $\rho_{\rm Kondo}\ll\rho_{\rm nor}$ gives back exactly the expression in Eq. (35).

In the numerical calculation, the integral in Eqs. (35) or (38) is replaced by a weighted sum with appropriate intervals. Introducing the integration variable x/α, the calculated Kondo resistivity depends only on t/α, which is shown in Figs. 10(a) and 10(b) for $S=2$ and $\frac{5}{2}$, respectively. Fitting the calculated Kondo resistivity for temperatures $T\gg T_K$ ($T=2-4$ K) by the function $\rho_{\rm Kondo}/\rho^{(0)}=-B_{\rm calc}\ln T$, as has been done in the experimental works (see Sec. VII), the behavior of $B_{\rm calc}$ was examined as a function of t/α, which can be seen in Fig. 11. To compare this calculated dependence of the coefficient B on the thickness to the experimental data, they were fitted by the function $B(t)=\rho^{(0)}B_{\rm calc}(t/\alpha)$, as shown in Fig. 12. The fitted value of α is $\alpha=247.7$ Å K, which is in agreement with the prediction given in I (Ref. 1) by Eq. (32) (see Sec. VII). The fit is not too sensitive to small changes ($<5\%$) in α.

If the sample is not thin, then the above results can be phenomenologically described in the framework of a simple model where the impurities in the region of the surface do not contribute to the Kondo resistivity, and outside that re-

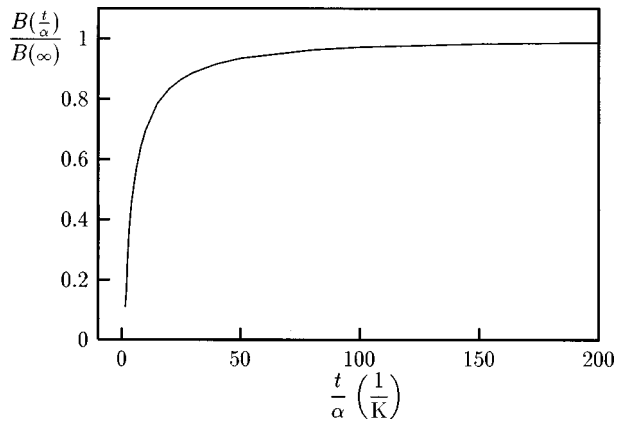

FIG. 11. The calculated coefficient B as a function of t/α. The Kondo temperature was chosen as $T_K=0.3$ K.

gion they are not affected. In this way the effective suppression length λ can be introduced, and then the average resistivity at low temperature ρ_t, e.g., for a thickness t:

$$\rho_t=\rho_{t=\infty}\frac{t-2\lambda}{t}. \tag{39}$$

According to this semiphenomenological formula, $B(t)=B_\infty(1-2\lambda/t)$, which was fitted to the experimental data. This can also be seen in Fig. 12, where the fitted value of the effective suppression layer parameter is $\lambda=207.5$ Å.

The effect of the mean free path in the ballistic region can be demonstrated directly by taking into account the effect of the mean free path in the anisotropy constant. We calculated the change of the electrical resistivity for a thin film with thickness $L=600$ Å, with anisotropy arising only at one of the surfaces in the forms

$$K=A\frac{l_{\mathrm{el}}}{d}, \tag{40a}$$

$$K=A\frac{l_{\mathrm{el}}}{d}e^{-d/l_{\mathrm{el}}}, \tag{40b}$$

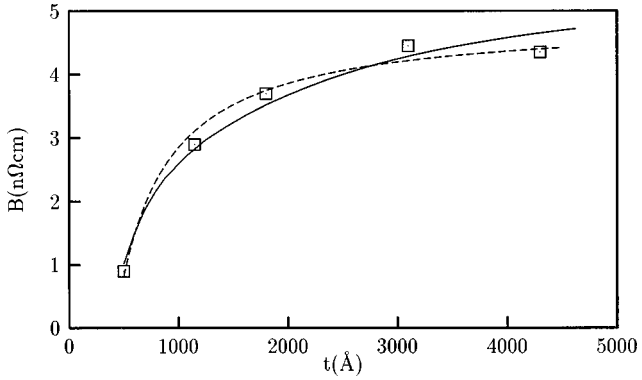

FIG. 12. Fit on the experimental data (squares) by the calculated formula $B(t)=\rho^{(0)}B_{\mathrm{calc}}(t/\alpha)$ (the Kondo temperature was chosen as $T_K=0.3$ K) with fitting parameters $\rho^{(0)}=20$ nΩ cm and $\alpha=247.7$ Å K (solid line), and by the phenomenological theory $B(t)=B_\infty(1-2\lambda/t)$ with fitting parameters $B_\infty=4.87$ nΩ cm and $\lambda=207.5$ Å (dashed line). The fit is not too sensitive to small changes ($<5\%$) in α.

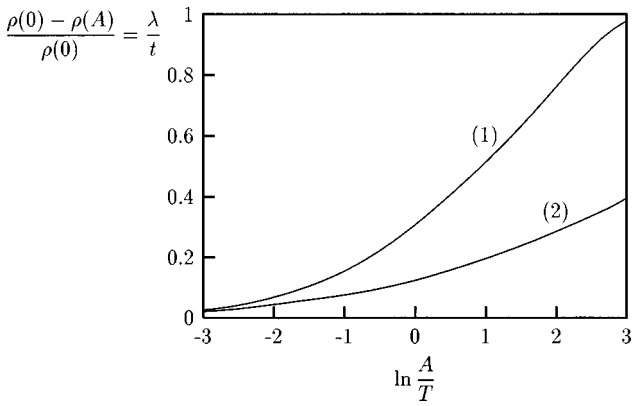

FIG. 13. The effect of the mean free path on the Kondo resistivity in the presence of anisotropy, arising from only one of the surfaces in a thin film with thickness $L=600$ Å, and elastic electron mean free path l_{el} for $S=2$ at $T=0.6$ K, (1) $K=A(l_{\mathrm{el}}/d)$, and (2) $K=A\,(l_{\mathrm{el}}/d)\,e^{-d/l_{\mathrm{el}}}$. The Kondo temperature was chosen as $T_K=0.3$ K.

where l_{el} is the elastic electron mean free path (e.g., $l_{\mathrm{el}}=100$ Å), d is the distance measured from the surface with an anisotropy of strength A, and the exponential decay is due to the mean free path. The electrical resistivity is calculated for $S=2$ at $T=2T_K$ just above the Kondo temperature T_K, as a function of the strength A of the anisotropy for two cases without and with an exponential factor [see Eq. (40)]. Increasing the anisotropy strength A, the spins are completely frozen in nearby the surface, but that region is limited by the finite mean free path. Figure 13 clearly demonstrates that the strength of the anisotropy and the size of the suppression layer are reduced due to the finite mean free path, as calculated by taking into account the anisotropy only for one of the surfaces.

VII. COMPARISON WITH EXPERIMENTS

In the last couple of years a very extensive study of the Kondo effect in thin films and wires has been performed. The experimental works concentrated on a determination of the effect of reduced dimensions on the Kondo temperature T_K, and the amplitude of the resistivity anomaly. A detailed critical discussion of the earlier works were given in Ref. 10. The early studies were performed by Giordano and co-workers,[11,12] and by DiTusa *et al.*[13] In order to discuss the effect of uncoupled magnetic impurities, only those experiments are listed which are performed in the dilute limit, thus e.g., for Au(Fe) alloys the Fe concentration is 30 ppm. These experiments belong to two groups depending on whether size effect was observed or not.

Concerning the theory, two regions must be distinguished. When the size of the sample (e.g., the thickness of the sample) is inside the ballistic region, then obviously the present theory must be applied. In the case of thicker samples, more care must be used. There is another theory by Martin, Wan, and Phillips,[14] which is applicable in the opposite limit of weak localization, where the disorder-induced depression or enhancement of the Kondo effect is predicted depending on the value of the spin-flip scattering rate τ_s^{-1} (depression is the case where T_K, $\hbar\tau_s^{-1}\ll T$). The competition between these theories needs further studies.

In the following, the discussion is organized according to different effects. First we discuss how the change in the density of states at the surface can influence the Kondo effect, but it is ruled out as an explanation of the size effects to be discussed, because it is applicable only on a much smaller scale (Sec. VII A). Then experiments with a considerable dependence on the size of the samples are discussed, and compared with the present theory (Sec. VII B). Finally those experiments are listed where no size effect was observed (Sec. VII C), or the concentrations of the impurities are in the spin-glass region (Sec. VII D).

A. Density-of-states effects

As been discussed in Sec. I of I,[1] size dependence cannot be expected just because the Kondo cloud cannot fully develop in all directions by reducing the size of the sample. The only possibility which was discussed by Zaránd[15] is that nearby the surface there is a change in the density of states of conduction electrons caused by formation of a Friedel-type oscillation due to the surface. That explanation was ruled out, because those changes in the density of states are very much localized in a few atomic distances measured from the surface, and the smallest sizes in the experiments to be discussed are about 300 Å. That effect may, however, show up in point-contact experiments, where the contact size is smaller by even more than one order of magnitude. Such experiments were performed by Yanson and co-workers[16–18] with Mn and Fe impurities in Cu contacts. Zaránd and Udvardi[19,20] showed that, depending on the actual position of the impurity, the density of states for an essential energy range around the Fermi surface can be enhanced or depressed by even 20%; thus $\rho=\rho_0+\delta\rho$, where $|\delta\rho/\rho_0|<0.2$. In order to demonstrate the effect, an energy-independent $\delta\rho$ is assumed, and for that case, in the expression of the Kondo temperature $T_K=D\sqrt{2J\rho_0}\exp[-1/2J(\rho_0+\delta\rho)]$ $=D\sqrt{2J\rho_0}\exp[-1/2J\rho_0]\exp[(2J\rho_0)^{-1}(\delta\rho/\rho_0)]$ there is an enhancement due to the second factor. Depending on the value of $(J\rho_0)^{-1}$, that enhancement can be over a factor of 100 for Mn and about 2–3 for Fe impurities. The enhancement is larger the smaller the Kondo temperature T_K.[16–18,20] In the experiments the enhancement is larger the smaller the contact size, thus to have a large enhancement most of the impurities must be nearby the surface. A similar effect was also seen[21] in point contacts with presumable tunneling two-level systems (TLS's), where an atom jumps between two positions and the orbital Kondo effect is developed[22,23] by coupling the conduction electrons with different angular momenta to the TLS's. As the typical sizes of the studied films and wires are much larger, and such a dominating enhancement of the Kondo temperature has never been observed, therefore this explanation can be ruled out.

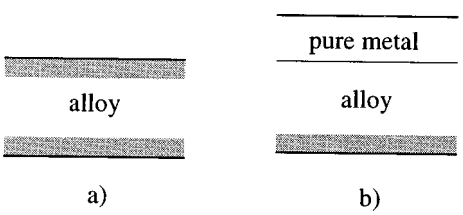

FIG. 14. Bilayer structure.

B. Experiments with observed size effect

Giordano and co-workers (for a review, see Ref. 10) performed a series of different experiments under different conditions, where the size effect was observed but the changes in the Kondo temperature were almost negligible. The experiments of different type are listed below.

1. Dependence on film thickness

The film experiments with thickness 265–1800 Å were performed, e.g., with 30-ppm Fe in Au, but similar results were also obtained for 100 ppm.[11,12] The resistivity was fitted by the formula

$$\rho(T)=\rho-B\ \ln(T), \tag{41}$$

where B is an adjustable parameter. It is well known for Kondo systems that B is just not the result of the first nonvanishing third-order perturbational result where B would be $B\sim J^3$, but it is the actual slope nearby or somewhat above the Kondo temperature (see, for example, Ref. 10). In the actual experiments the temperature range 1.8–4 K was studied, while $T_K=0.3$ K. The dependence of that coefficient B on thickness was plotted as shown in Fig. 12. The experimental results are fitted by the calculated dependence of B on the thickness with parameter $\alpha=247.7$ Å K, and by the semiphenomenological formula given by Eq. (39) with the effective suppression layer parameter value $\lambda=207.5$ Å in Fig. 12.[24,25] That value of α is in agreement with the estimate given in I (Ref. 1) by Eq. (32). There was not any signal of an essential change in the Kondo temperature,[10] in agreement with our theoretical result. It is interesting to note that the estimated Kondo coherence length was about 3×10^4 Å, much larger than the thickness of the sample. Similar experiments were performed with wires where more geometrical effects are expected, and the results are qualitatively similar but not identical. The simple semiphenomenological formula given by Eq. (39) is not appropriate in those cases. Qualitatively very similar results were reported in Ref. 26 but there are quantitative differences very likely due to the sample preparation.

2. Kondo proximity effect

A set of experiments[27,28] was performed where the film of dilute alloys was covered by a second layer of pure metal. The observation was that, in the case of a thin layer of dilute alloys with a significant suppression of the Kondo effect, the covering by a second pure film results in a partial recovery of that suppression. In Fig. 14, with the suppression layers indicated, it is shown that the bilayer structure has a suppression layer only on one side of the film of dilute alloys; thus only one half of the suppression is expected. In order to verify the importance of the role of the spin-orbit interaction in the superimposed layer to complete the neighborhood of the impurity with a uniform spin-orbit coupling, we suggest experiments where the superimposed layer has negligible spin-orbit interaction (e.g., Al or Mg). In that case the boundary is changed, but the anisotropy should remain.

3. Kondo proximity effect with overlayers with different disorder

It has been shown experimentally[29] that the Kondo resistivity suppression in a film of dilute alloys covered by a pure

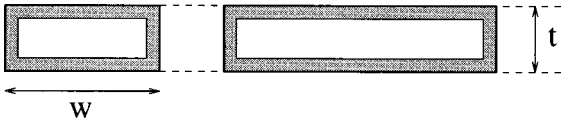

FIG. 15. Stripes with the same thickness t and changing width w.

film but with different disorder depends on the disorder in the overlayer. It was found that the larger the disorder the smaller the recovery is. As discussed above, if the thickness of the overlayer and the mean free path l_{el} in it are larger than the thickness of the suppression layer λ, then the depression takes place only on one side of the film of dilute alloys. On the other hand, if the pure overlayer contains disorder, then the electron entering that overlayer cannot bring back information to the magnetic impurity by their momenta, as their momenta is changed in the overlayer (the overlayer is not in the ballistic regime). In these cases the reduction in the anisotropy is only partially developed, as the surroundings of the impurity are not perfectly spherical, in contrast to the case of an overlayer with long mean free path.

C. Experiments without size effect

In contrast to the measurements discussed in Sec. VII B, there is a series of experiments by Chandrasekhar *et al.*[30] in which the size dependence was not found. The geometries of these experiments were different, the thickness of the sample t was kept the same ($t=380$ Å), but the width of the stripes w was changed between 380 and 10^6 Å (see Fig. 15). After the correction due to weak-localization effects and to electron-electron interaction, no size dependence was claimed. On the basis of the present theory, for samples $t \ll w$, no size dependence is expected, as the ratio of the volume of the suppression layers to the total volume is not changing. Where $t \sim w$, the anisotropy due to the geometry becomes more complicated, thus it is hard to make a comparison with the present theory. On the other hand, for $t \sim w$ the experimental points fall off somewhat from the main averaged line; that, of course, may be due to experimental errors. According to the present theory the averaged Kondo resistivity for $w \gg t$ had to be smaller than the bulk resistivity, but this seems to be not the case.[31] Finally, it should be mentioned that no size effect was observed studying $La_{1-x}Ce_x$ films, where Ce has $S=\frac{1}{2}$, for which no surface anisotropy is expected.[32]

D. Higher concentration

There are several experiments[13,33] with higher impurity concentrations. In these cases the impurity-impurity interaction mediated by the RKKY interaction competes with the Kondo effect. In another set of experiments,[13] the thickness of the film was changed in samples made of Cu with 1000 ppm Cr, and a very similar depression of the Kondo effect, as described above in Sec. VII B, was found. Wires with geometries similar to those discussed in Sec. VII C, but with 2800 ppm impurities, do not show a dependence on the width d,[33] but the overall amplitude is substantially suppressed compared to the bulk, which was attributed to spin-glass effects.

VIII. CONCLUSION

In the present paper, the influence of the spin-orbit induced surface anisotropy is studied on the Kondo effect in dilute magnetic alloys samples of finite size at least in one dimension. That anisotropy splits the energy levels for an impurity spin $S>\frac{1}{2}$. That anisotropy reduces as the bulk part of the sample is approached relatively slowly as $1/d$, where d is the distance of the impurity measured from the surface. That anisotropy occurs for samples of any shape, but for those cases further theories should be developed. The range where the anisotropy is relevant can be characterized by the suppression length λ introduced in Sec. VI, which is proportional to the strength of the anisotropy but limited by the mean free path of the electron as the anisotropy reflects the presence of the surface in the ballistic region nearby the impurity. Thus that suppression length cannot exceed a few hundred Å, in accordance with the experiments discussed in Sec. VII B.

That anisotropy hinders the motion of the impurity spin S if $S>\frac{1}{2}$ and the Kondo effect is affected in those regions of the samples where the anisotropy is not negligible relative to the Kondo temperature T_K. In order to calculate the Kondo resistivity, the renormalized exchange coupling constants are calculated in Secs. III and IV by using the multiplicative renormalization-group technique which is applicable only for temperatures T larger than the Kondo temperature T_K; thus no detailed prediction can be made outside that region. It can be accepted, however, that if the Kondo effect is already reduced in the region $T>T_K$,[9] similar effect is also expected for $T<T_K$. The resistivity is calculated by solving the Boltzmann equation in Sec. V for integer and half-integer spins with different anisotropy strengths. Even if the calculated resistivity curves in Figs. 9(a) and 9(b) show different characteristic features by developing a resistivity maxima at different temperatures and of different amplitudes, these features are smeared out as an average over the strength of the anisotropy is taken for $T>T_K$. The curves calculated for thin films (see Fig. 10) show a smooth increase of the resistivity. More structures could be expected only in those experiments where the impurities are at a in certain distance measured from the surface. If the anisotropy does not dominate the complete sample, then, as the result of the average taken, the largest resistivity slope as a function of temperature is in the region of the Kondo temperature T_K, and its position cannot be shifted too much on the scale of the Kondo temperature T_K. That theoretical result is in accordance with the experimental findings (see Sec. VII B).

The relatively weak sensitivity of the observed region of the largest resistivity slope on the size of the samples rules out the density state effects nearby the surface, in contrast to the point-contact experiments (see Sec. VII A). The size dependence associated with the large Kondo compensation cloud is not observed, in agreement with the Kondo theory where such a simple connection is ruled out.

The calculated Kondo resistivity for thin films was fitted for temperatures $T \gg T_K$ ($T=2-4$ K) by the function $\rho_{\text{Kondo}}/\rho^{(0)} = -B_{\text{calc}} \ln T$, which is compared to the experimental data in Fig. 12 and gives excellent agreement. The phenomenological theory using the effective suppression length λ (see Sec. VI) works remarkably well to interpret

qualitatively the experimental data quoted in Sec. VII. The fit of the experimental data is shown in Fig. 12. The different proximity effects described in Sec. VII B can be also well explained by the present theory.

It is important that the role of mean free path (Sec. VI; see Fig. 13) reduces the effect of the large anisotropy constant; thus for a large range of strong anisotropy the size dependence remains in a limited range as long as the elastic mean free paths are in the same order of magnitude. In this way the size effect can be comparable for different host materials with different large spin-orbit interactions but with comparable elastic mean free paths.

We have to emphasize, however, that our calculation does not consider the localization effects which are present in samples of larger sizes. Such effects have recently been predicted by Martin, Wan, and Phillips,[14] and deserve further detailed studies. In addition to those localization effects, the theoretical studies must be extended to the microscopic calculations of the anisotropy constant.

Considering further experiments, the mean free path effects should be studied. The most relevant experiment to verify the role of the spin-orbit interaction directly could be the proximity experiments, where the superimposed layer is made of another metal without spin-orbit interaction, as discussed in Sec. VII B. In those cases the uniform surrounding of the impurity would not be developed; thus the anisotropy remains. Furthermore, experiments with impurities at a certain distance measured from the surface would be also very instructive. Summarizing, the presented theory is able to provide a coherent description of the size effects of the Kondo resistivity in thin films, which is not related to the size of the Kondo compensation cloud in any sense.

ACKNOWLEDGMENTS

The present authors are grateful for useful discussions with G. Bergmann, L. Borda, N. Giordano, B. L. Gyorffy, H. v. Löhneysen, Ph. Nozières, M. Parpia, P. Phillips, J. Sólyom, L. Szunyogh, I. K. Yanson, and G. Zaránd. The work was supported by Hungarian Grant Nos. OTKA T02228-T021228/1996 and T024005/1997. One of us (O. Ú.) was supported by TEMPUS Mobility Grant, and A. Z. is grateful for the support by the Humboldt Foundation.

APPENDIX

Here we calculate the second- and third-order vertex corrections, and the second-order self-energy correction for the impurity spin shown in Figs. 5 and 6, respectively.

Carrying out Matsubara's summation and analytical continuation, changing the integrals $\int(d^3k/(2\pi)^3)$ to $\int\rho(\varepsilon)d\varepsilon\int(d\Omega_k/4\pi)$ and using the assumption for $\rho(\varepsilon)$ in Sec. I, the contribution of the second-order diagrams are

$$\begin{aligned} &J_{MM''}J_{M''M'}(\sigma^i\sigma^j)_{\sigma\sigma'}S^i_{MM''}S^j_{M''M'}\rho_0 \\ &\quad\times\int_{-D}^{D}d\varepsilon\frac{1-n_F(\varepsilon)}{\varepsilon-\omega+K_{M''}-K_M} \\ &\quad+J_{MM''}J_{M''M'}(\sigma^j\sigma^i)_{\sigma\sigma'}S^i_{MM''}S^j_{M''M'}\rho_0 \\ &\quad\times\int_{-D}^{D}d\varepsilon\frac{n_F(\varepsilon)}{\varepsilon-\omega+K_{M'}-K_{M''}} \end{aligned} \tag{A1}$$

for diagrams corresponding to Fig. 5(a). The third-order diagrams' contributions are

$$\begin{aligned} &-(\sigma^i\sigma^j\sigma^k)_{\sigma\sigma'}J_{MN}J_{NN'}J_{N'M'}S^i_{MN}S^j_{NN'}S^k_{N'M'}\rho_0^2 \\ &\quad\times\int_{-D}^{D}\frac{[1-n_F(\varepsilon)d\varepsilon]}{\omega-\varepsilon+K_M-K_N}\int_{-D}^{D}\frac{[1-n_F(\varepsilon')]d\varepsilon'}{\omega-\varepsilon'+K_M-K_{N'}} \\ &\quad-(\sigma^k\sigma^j\sigma^i)_{\sigma\sigma'}J_{MN}J_{NN'}J_{N'M'} \\ &\quad\times S^i_{MN}S^j_{N'M'}S^k_{NN'}\rho_0^2S^i_{MN}S^j_{NN'}S^k_{N'M'}\rho_0^2 \\ &\quad\times\int_{-D}^{D}\frac{n_F(\varepsilon)d\varepsilon}{\varepsilon-\omega+K_{M'}-K_N}\int_{-D}^{D}\frac{n_F(\varepsilon')d\varepsilon'}{\varepsilon'-\omega+K_{M'}-K_{N'}} \end{aligned} \tag{A2}$$

for diagrams corresponding to Fig. 5(b),

$$\begin{aligned} &-Tr(\sigma^i\sigma^j)\sigma^k_{\sigma\sigma'}J_{MN}J_{NN'}J_{N'M'}S^i_{MN}S^j_{N'M'}S^k_{NN'}\rho_0^2 \\ &\quad\times\int_{-D}^{D}\int_{-D}^{D}\frac{n_F(\varepsilon)[1-n_F(\varepsilon')]d\varepsilon d\varepsilon'}{(\varepsilon-\varepsilon'+K_M-K_N)(\varepsilon-\varepsilon'+K_{M'}-K_{N'})} \end{aligned} \tag{A3}$$

for diagrams corresponding to Fig. 5(c), and

$$\begin{aligned} &(\sigma^i\sigma^j\sigma^k)_{\sigma\sigma'}J_{MN}J_{NN'}J_{N'M'}S^j_{MN}S^i_{NN'}S^k_{N'M'}\rho_0^2\int_{-D}^{D}\int_{-D}^{D}\frac{n_F(\varepsilon)[1-n_F(\varepsilon')]d\varepsilon d\varepsilon'}{(\omega-\varepsilon'+K_M-K_{N'})(\varepsilon-\varepsilon'+K_M-K_N)} \\ &+(\sigma^k\sigma^j\sigma^i)_{\sigma\sigma'}J_{MN}J_{NN'}J_{N'M'}S^j_{MN}S^i_{NN'}S^k_{N'M'}\rho_0^2\int_{-D}^{D}\int_{-D}^{D}\frac{[1-n_F(\varepsilon)]n_F(\varepsilon')d\varepsilon d\varepsilon'}{(\varepsilon'-\omega+K_{M'}-K_{N'})(\varepsilon'-\varepsilon+K_M-K_N)} \\ &+(\sigma^i\sigma^j\sigma^k)_{\sigma\sigma'}J_{MN'}J_{N'N}J_{NM'}S^i_{MN}S^k_{NN'}S^j_{N'M'}\rho_0^2\int_{-D}^{D}\int_{-D}^{D}\frac{n_F(\varepsilon)[1-n_F(\varepsilon')]d\varepsilon d\varepsilon'}{(\omega-\varepsilon'+K_M-K_N)(\varepsilon-\varepsilon'+K_{M'}-K_{N'})} \\ &+(\sigma^k\sigma^j\sigma^i)_{\sigma\sigma'}J_{MN'}J_{N'N}J_{NM'}S^i_{MN}S^k_{NN'}S^j_{N'M'}\rho_0^2\int_{-D}^{D}\int_{-D}^{D}\frac{[1-n_F(\varepsilon)]n_F(\varepsilon')d\varepsilon d\varepsilon'}{(\varepsilon'-\omega+K_{M'}-K_N)(\varepsilon'-\varepsilon+K_{M'}-K_{N'})} \end{aligned} \tag{A4}$$

for diagrams corresponding to Fig. 5(d).

The second-order correction to the self-energy for the impurity spin according to Fig. 6 is

$$-Tr(\sigma^i\sigma^j)J_{MM'}J_{M'M}S^i_{MM'}S^j_{M'M}\rho_0^2 \times\int_{-D}^{D}d\varepsilon\int_{-D}^{D}d\varepsilon'\,\frac{[1-n_F(\varepsilon)]n_F(\varepsilon')}{\varepsilon-\varepsilon'-\tilde{\omega}+K_{M'}-K_M}. \tag{A5}$$

For the same indices, summation must be carried out.

The spin factors in Eqs. (A1), (A2), (A3), (A4), and (A5) were calculated by using the identities

$$(\sigma^i\sigma^j)_{\sigma\sigma'}=\delta_{ij}\delta_{\sigma\sigma'}+i\varepsilon_{ijk}\sigma^k_{\sigma\sigma'}, \tag{A6a}$$

$$(\sigma^i\sigma^j\sigma^k)_{\sigma\sigma'}=\delta_{ij}\sigma^k_{\sigma\sigma'}+\delta_{jk}\sigma^i_{\sigma\sigma'}-\delta_{ik}\sigma^j_{\sigma\sigma'}+i\varepsilon_{ijk}\delta_{\sigma\sigma'}, \tag{A6b}$$

introducing the $S^{\pm}$ operators in a usual way, and exploiting that their matrix elements are

$$S^+_{MM'}=p(S,M')\,\delta_{M,M'+1}=\sqrt{S(S+1)-M'(M'+1)}\,\delta_{M,M'+1}, \tag{A7a}$$

$$S^-_{MM'}=q(S,M')\,\delta_{M,M'-1}=\sqrt{S(S+1)-M'(M'-1)}\,\delta_{M,M'-1}. \tag{A7b}$$

Turning to the integrals in Eqs. (A1), (A2), (A3), (A4), and (A5), after changing the integration variable in integrals containing $[1-n_F(\varepsilon)]$ or $[1-n_F(\varepsilon')]$ from ε (ε') to $-\varepsilon$ ($-\varepsilon'$), they were evaluated in a logarithmic approximation. The integrals in Eq. (A1) give the logarithmic contributions

$$I^{(1)}_{MM''}(D)=\int_{-D}^{D}d\varepsilon\frac{n_F(\varepsilon)}{\varepsilon+\omega+K_M-K_{M''}} \approx\ln\left|\frac{\omega+K_M-K_{M''}}{D}\right|+I(\omega+K_M-K_{M''}) \tag{A8}$$

for $D>|\omega+K_M-K_{M''}|$, and

$$I^{(2)}_{M'M''}(D)=\int_{-D}^{D}d\varepsilon\frac{n_F(\varepsilon)}{\varepsilon-\omega+K_{M'}-K_{M''}} \approx\ln\left|\frac{\omega-K_{M'}+K_{M''}}{D}\right|+I(\omega-K_{M'}+K_{M''}) \tag{A9}$$

for $D>|-\omega+K_{M'}-K_{M''}|$.

The integral in Eq. (A5) gives the logarithmic contribution

$$I^{(3)}_{MM'}(D)=\int_{-D}^{D}d\varepsilon\int_{-D}^{D}d\varepsilon'\,\frac{n_F(\varepsilon)n_F(\varepsilon')}{\varepsilon+\varepsilon'+\tilde{\omega}-\lambda+K_M-K_{M'}} \approx(\tilde{\omega}-\lambda+K_M-K_{M'})\ln\left|\frac{\tilde{\omega}-\lambda+K_M-K_{M'}}{D}\right| \tag{A10}$$

for $D>|\tilde{\omega}-\lambda+K_M-K_{M'}|$.

The integrals in Eq. (A2) give the logarithmic contributions

$$I^{(4)}_{MNN'}(D)=I^{(1)}_{MN}(D)I^{(1)}_{MN'}(D) \approx\left(\ln\left|\frac{\omega+K_M-K_N}{D}\right|+I(\omega+K_M-K_N)\right) \times\left(\ln\left|\frac{\omega+K_M-K_{N'}}{D}\right|+I(\omega+K_M-K_{N'})\right) \tag{A11}$$

for $D>|\omega+K_M-K_N|$ and $D>|\omega+K_M-K_{N'}|$ and

$$I^{(5)}_{M'NN'}(D)=I^{(2)}_{M'N}(D)I^{(2)}_{M'N'}(D) \approx\left(\ln\left|\frac{\omega-K_{M'}-K_N}{D}\right|+I(-\omega+K_M-K_N)\right) \times\left(\ln\left|\frac{\omega-K_{M'}-K_{N'}}{D}\right|+I(-\omega+K_{M'}-K_{N'})\right) \tag{A12}$$

for $D>|-\omega+K_{M'}-K_N|$ and $D>|-\omega+K_M-K_{N'}|$.

The integral in Eq. (A3) gives the logarithmic contributions for $M\neq N$, $M'\neq N'$, and $K_{M'}-K_{N'}-K_M+K_N\neq 0$:

$$I^{(6)}_{MNM'N'}(D)=\int_{-D}^{D}d\varepsilon\int_{-D}^{D}d\varepsilon' \times\frac{n_F(\varepsilon)n_F(\varepsilon')}{(\varepsilon+\varepsilon'+K_M-K_N)(\varepsilon+\varepsilon'+K_{M'}-K_{N'})} \approx\frac{K_M-K_N}{K_{M'}-K_{N'}-K_M+K_N}\ln\left|\frac{K_M-K_N}{D}\right| -\frac{K_{M'}-K_{N'}}{K_{M'}-K_{N'}-K_M+K_N}\ln\left|\frac{K_{M'}-K_{N'}}{D}\right| \tag{A13}$$

for $D>|K_M-K_N|$ and $D>|K_{M'}-K_{N'}|$. For $K_{M'}-K_{N'}=K_M-K_N\neq 0$,

$$I^{(6)}_{MNM'N'}(D)\approx-\ln\left|\frac{K_M-K_N}{D}\right| \tag{A14}$$

for $D>|K_M-K_N|$. Also,

$$I^{(6)}_{MMM'M'}(D)\approx-\ln\left|\frac{T}{D}\right|. \tag{A15}$$

The integrals in Eq. (A4) give the logarithmic contributions

$$I^{(7)}_{MN'MN}(D)=\int_{-D}^{D}d\varepsilon\int_{-D}^{D}d\varepsilon' \times\frac{n_F(\varepsilon)n_F(\varepsilon')}{(\varepsilon'+\omega+K_M-K_{N'})(\varepsilon+\varepsilon'+K_M-K_N)} \approx\frac{1}{2}\ln^2\left|\frac{\omega+K_M-K_{N'}}{D}\right|+I(\omega+K_M-K_{N'}) \times\ln\left|\sqrt{\frac{(K_M-K_N)^2+T^2}{D}}\right| \tag{A16}$$

for $D>|\omega+K_M-K_{N'}|$ and $D>\sqrt{(K_M-K_N)^2+T^2}$, where T is the temperature;

$$I^{(8)}_{M'N'MN}(D)=\int_{-D}^{D}d\varepsilon\int_{-D}^{D}d\varepsilon' \times\frac{n_F(\varepsilon)n_F(\varepsilon')}{(\varepsilon'-\omega+K_{M'}-K_{N'})(\varepsilon+\varepsilon'+K_M-K_N)} \approx\frac{1}{2}\ln^2\left|\frac{-\omega+K_{M'}-K_{N'}}{D}\right| +I(-\omega+K_{M'}K_{N'}) \times\ln\left|\sqrt{\frac{(K_M-K_N)^2+T^2}{D}}\right| \tag{A17}$$

for $D>|-\omega+K_{M'}-K_{N'}|$ and $D>\sqrt{(K_M-K_N)^2+T^2}$;

$$I^{(9)}_{MNM'N'}(D)=\int_{-D}^{D}d\varepsilon\int_{-D}^{D}d\varepsilon' \times\frac{n_F(\varepsilon)n_F(\varepsilon')}{(\varepsilon'-\omega+K_M-K_N)(\varepsilon+\varepsilon'+K_{M'}-K_{N'})} =I^{(7)}_{MNM'N'}(D); \tag{A18}$$

and

$$I^{(10)}_{M'NM'N'}(D)=\int_{-D}^{D}d\varepsilon\int_{-D}^{D}d\varepsilon' \times\frac{n_F(\varepsilon)n_F(\varepsilon')}{(\varepsilon'-\omega+K_{M'}-K_N)(\varepsilon+\varepsilon'+K_{M'}-K_{N'})} =I^{(8)}_{M'NM'N'}(D). \tag{A19}$$

In the estimations above, the function $I(\alpha)=\int_0^\infty d\varepsilon\, n_F(\varepsilon)[2\varepsilon/(\varepsilon^2-\alpha^2)]$ was introduced which is related to the finite-T divergences. From the scaling equations, the $I(\alpha)$ function is canceled out. For the sake of handling these contributions more comfortably, $\omega,\tilde{\omega}\sim T$ were set in the arguments of the logarithms in a way that substituted $\omega+a$ $(\tilde{\omega}+a)$ with $\sqrt{a^2+T^2}$.

[1] O. Újsághy and A. Zawadowski, preceding paper, Phys. Rev. B **57**, 11 598 (1998).
[2] O. Újsághy, A. Zawadowski, and B. L. Gyorffy, Phys. Rev. Lett. **76**, 2378 (1996).
[3] O. Újsághy and A. Zawadowski, in *Proceedings of the XXXIst Rencontres de Moriond, Correlated Fermions and Transport in Mesoscopic Systems, Les Arcs, Savoie, France, January 20–27* (Moriond, Paris, 1996), p. 535.
[4] Shin-ichi Kashiba *et al.*, J. Phys. Soc. Jpn. **55**, 1341 (1986).
[5] A. A. Abrikosov, Physics (Long Island City, NY) **2**, 5 (1965).
[6] M. Fowler and A. Zawadowski, Solid State Commun. **9**, 471 (1971).
[7] See, for example A. Abrikosov, L. P. Gorkov, and I. E. Dzyaloshinski, *Methods of Quantum Field Theory in Statistical Physics* (Dover, Inc., New York, 1975).
[8] J. Sólyom, J. Phys. F **4**, 2269 (1974).
[9] See, for example, Kei Yoshida, Phys. Rev. **107**, 396 (1957).
[10] M. A. Blachly and N. Giordano, Phys. Rev. B **51**, 12537 (1995).
[11] G. Chen and N. Giordano, Physica B **165-166**, 455 (1990).
[12] G. Chen and N. Giordano, Phys. Rev. Lett. **66**, 209 (1991).
[13] J. F. DiTusa, K. Lin, M. Park, M. S. Isaacson, and M. Parpia, Phys. Rev. Lett. **68**, 678 (1992).
[14] I. Martin, Yi Wan, and Philip Phillips, Phys. Rev. Lett. **78**, 114 (1997).
[15] G. Zaránd, Diploma Thesis at the Eotvos University of Budapest, 1992 (unpublished).
[16] I. K. Yanson *et al.*, Fiz. Nizk. Temp. **20**, 1062 (1994) [Low Temp. Phys. **20**, 836 (1994)].
[17] I. K. Yanson, V. V. Fisun, R. Hesper, A. V. Khotkevick, J. M. Krans, J. A. Mydosh, and J. M. van Ruitenbeek, Phys. Rev. Lett. **74**, 302 (1995).
[18] N. van der Post, F. L. Mettes, J. A. Mydosh, J. M. van Ruitenbeek, and I. K. Yanson, Phys. Rev. B **53**, R476 (1996).
[19] G. Zaránd and L. Udvardi, Physica B **218**, 68 (1996).
[20] G. Zaránd and L. Udvardi, Phys. Rev. B **54**, 7606 (1996).
[21] R. J. Keijsers, O. Shklyarevskii, and H. van Kempen, Phys. Rev. B **51**, 5628 (1995).
[22] A. Zawadowski, Phys. Rev. Lett. **45**, 211 (1980).
[23] See for a review D. Cox and A. Zawadowski, cond-mat/9704103v2 [Adv. Phys. (to be published)].
[24] M. A. Blachly and N. Giordano, Phys. Rev. B **46**, 2951 (1992).
[25] M. A. Blachly and N. Giordano, Phys. Rev. B **49**, 6788 (1994).
[26] G. Apostopoulos and C. Papastaikoudis, Solid State Commun. **99**, 277 (1996).
[27] M. A. Blachly and N. Giordano, Physica B **194-196**, 983 (1994).
[28] M. A. Blachly and N. Giordano, Phys. Rev. B **49**, 6788 (1994).
[29] M. A. Blachly and N. Giordano, Europhys. Lett. **27**, 687 (1994).
[30] V. Chandrasekhar, P. Santhanam, N. E. Penebe, R. A. Webb, H. Vloeberghs, C. H. Van Haesendock, and Y. Bruynseraede, Phys. Rev. Lett. **72**, 2053 (1994).
[31] V. Chandrasekhar (private communication).
[32] C. Roth, C. Sürgersand, and H. v. Löhneysen, Phys. Rev. B **54**, 3454 (1996).
[33] G. Neuttiens *et al.*, Europhys. Lett. **34**, 623 (1996).